

Formation of L₁₂ modified Al_{2.5}Cu_{0.5}Ti phase by heat treatment of spark-plasma-sintered Cu/Al₃Ti specimens

Yoshimi Watanabe^{1*}, Kazuaki Hirata², and Hisashi Sato¹

¹Department of Physical Science and Engineering, Graduate School of Engineering, Nagoya Institute of Technology, Nagoya 466-8555, Japan

²Department of Engineering Physics, Electronics and Mechanics, Graduate School of Engineering, Nagoya Institute of Technology, Nagoya 466-8555, Japan

*E-mail: yoshimi@nitech.ac.jp

In our previous studies, the influence of L₁₂ modified Al_{2.5}Cu_{0.5}Ti and Al_{2.7}Fe_{0.3}Ti particles on the grain refining performance of an Al cast was studied. It has been shown that the L₁₂ modified intermetallic compound particles act as heterogeneous nucleation sites of α -Al solidification. Since nuclei are formed on the surface of the heterogeneous nucleation site particles, only the surface region of the Al₃Ti particles must be modified into an L₁₂ structure. In this study, therefore, the formation of the Al_{2.5}Cu_{0.5}Ti phase by the reaction between Al₃Ti and Cu is studied. For this purpose, Cu/Al₃Ti diffusion couple specimens and specimens of Al₃Ti particles dispersed in a Cu matrix are fabricated by a spark plasma sintering (SPS) method, and the reaction between Cu and Al₃Ti during heat treatment of these specimens is studied. It is found that the L₁₂ modified Al_{2.5}Cu_{0.5}Ti phase is formed at the Cu/Al₃Ti interface by heat treatment.

1. Introduction

The equiaxed grain structure of Al alloy castings ensures uniform mechanical properties, reduced ingot cracking, improved feeding to eliminate shrinkage porosity, distribution of secondary phases and microporosity on a fine scale, and improved machinability and cosmetic features.¹⁾ As one of the methods of obtaining the equiaxed grain structure of Al alloy castings, the addition of refiners, such as Al-Ti, Al-Ti-B, and Al-Ti-C system alloys, has been carried out.¹⁻⁹⁾ In these refiners, the Al_3Ti , TiB_2 , and TiC particles act as heterogeneous nucleation sites of α -Al solidification. Among them, we have discussed the importance of Al_3Ti particles.^{8,9)} It is well accepted that effective heterogeneous nucleation sites have a good lattice registry with a solidified Al matrix; here, solidified Al has the fcc structure with $a = 0.4049$ nm.¹⁰⁾ On the other hand, Al_3Ti has a low-symmetry tetragonal D_{022} structure and its lattice parameters are $a = 0.3851$ nm and $c = 0.8608$ nm.¹¹⁾ Therefore, different orientation relationships result in different lattice registry values.¹²⁻¹⁴⁾

It is known that, upon the replacement of some of the Al atoms with Cu, Fe, Ni, Cr, or Zn, the crystal structure changes from the unfavorable low-symmetry tetragonal D_{022} structure to the L_{12} structure.¹⁵⁻²⁰⁾ Moreover, by changing the replacing element, the lattice constant of L_{12} phases is controllable. In our previous studies, the effects of L_{12} modified intermetallic compound particles, such as $\text{Al}_{2.5}\text{Cu}_{0.5}\text{Ti}$ ²¹⁾ and $\text{Al}_{2.7}\text{Fe}_{0.3}\text{Ti}$ ^{22,23)}, on the grain refining performance of an Al cast were studied. It has been shown that L_{12} modified intermetallic compound particles act as heterogeneous nucleation sites of α -Al solidification. Since nuclei are formed on the surface of heterogeneous nucleation site particles, only the surface region of the particles must be modified into the L_{12} structure. Therefore, there is a need to fabricate an L_{12} modified intermetallic compound not by melting Al, Ti, and replacement elements but by the reaction between Al_3Ti and replacement elements. Figure 1 shows an Al-Ti-Cu ternary alloy phase diagram.²⁴⁾ As can be seen, the $\text{Al}_{2.5}\text{Cu}_{0.5}\text{Ti}$ region is located between Al_3Ti and Cu. Therefore, it is expected that the reaction between Al_3Ti and Cu forms the L_{12} modified $\text{Al}_{2.5}\text{Cu}_{0.5}\text{Ti}$ phase.

On the basis of the above background, in this study, the reaction between Al_3Ti and Cu is studied using two sets of specimens. One is a Cu/ Al_3Ti diffusion couple specimen, because the diffusion couple made up of two metals is frequently used to determine the number of intermetallic phases in an equilibrium phase diagram.²⁵⁾ The other one has

Al_3Ti particles dispersed in a Cu matrix. These specimens are fabricated by a spark plasma sintering (SPS) method, where SPS simultaneously applies a pulsed current and a uniaxial pressure to the punches of a mold system loaded with a mixture of powders to be sintered.²⁶⁾ The SPS method can also be used for solid-state bonding between similar or dissimilar materials.²⁷⁾ SPS can be carried out at a low temperature with short heating, holding, and cooling times^{28,29)}, which can be achieved in a non-equilibrium state. The Cu/ Al_3Ti diffusion couple specimen and Al_3Ti particle dispersed specimen are heat-treated at elevated temperatures, and the reaction between Al_3Ti and Cu is studied.

2. Experimental methods

2.1 Cu/ Al_3Ti diffusion couple specimen

Firstly, the button-shaped Al_3Ti intermetallic compound was prepared by an arc melting method in argon atmosphere, as shown in Fig. 2(a). The button-shaped Al_3Ti intermetallic compound was homogenized at 1100 °C for 4 h, as shown in Fig. 2(b), and then crushed into fine particles with a hammer, as shown in Fig. 2(c). Hereafter, the particles prepared by the crushing of an arc-melted Al_3Ti intermetallic compound will be denoted as “crushed particles”. The crushed particles were sieved to obtain particle sizes of 75–150 μm , as shown in Fig. 2(d). Then, a bulk Al_3Ti sample of 20 mm diameter and 5 mm height was fabricated by SPS, as shown in Fig. 2(e). Sintering using an SPS apparatus (SPS Syntex SPS-515S) was performed at 900 °C under an applied stress of 30 MPa. A bulk Cu sample of 20 mm diameter and 5 mm height was also prepared from Cu powder [Fig. 2(f)] by SPS at 800 °C under an applied stress of 30 MPa, as shown in Fig. 2(g). The surfaces for bonding were ground with emery paper and polished with a 1 μm alumina suspension. By using these bulk Al_3Ti and Cu samples, a Cu/ Al_3Ti diffusion couple specimen was fabricated by SPS at 600, 700, and 800 °C, as shown in Fig. 2(h). The Cu/ Al_3Ti diffusion couple specimen fabricated by SPS at 600 °C for 300 s was heated at 600 °C for 0.5, 1, 2, 4, and 8 h.

2.2 Specimen with Al_3Ti particles dispersed in Cu matrix

The specimen with Al_3Ti particles dispersed in the Cu matrix (Cu-10 vol% Al_3Ti specimen) was fabricated similarly to the Al-10 vol% $\text{Al}_{2.5}\text{Cu}_{0.5}\text{Ti}$ refiner²¹⁾ and Al-10 vol% $\text{Al}_{2.7}\text{Fe}_{0.3}\text{Ti}$ refiner^{22,23)} reported in previous studies. Two types of Al_3Ti particles are used. One is

crushed particles and the other is gas-atomized particles prepared by a gas atomization method. The sieved Al_3Ti particles of 150-250 μm diameter are mixed with pure Cu particles (99.5%, 25 μm), where the volume fraction of Al_3Ti particles was fixed to 10 vol%. The above mixed particles were sintered by SPS at 500, 600, and 700 $^\circ\text{C}$ for 300 s under an applied stress of 30 MPa. The specimens with crushed and gas-atomized Al_3Ti particles dispersed in the Cu matrix will be denoted as “crushed particle dispersed specimen” and “gas-atomized particle dispersed specimen”, respectively. The crushed particle dispersed specimen and the gas-atomized particle dispersed specimen were heat-treated at 600 $^\circ\text{C}$ for 0.5, 1, 2, 4, and 8 h.

2.3 Evaluation of microstructures

A scanning electron microscopy (SEM; JEOL JSM-5900LV) apparatus equipped with an energy dispersive X-ray spectrometer (EDS; JEOL JED-2200) was employed to examine the microstructures and determine the chemical compositions of Al, Ti, and Cu elements around the Cu/ Al_3Ti interface. An X-ray diffraction (XRD; Rigaku RINT-2100) apparatus with copper $\text{K}\alpha$ radiation was used to identify the crushed particles and gas-atomized particles. However, XRD analysis is not the best way to identify the crystal structure of the reaction phases, since their thickness is extremely narrow. In addition, observation by transmission electron microscopy (TEM) would also be difficult for these specimens, since the technique requires thinning at the interface. Alternatively, the crystal structure of the reaction phases at the Cu/ Al_3Ti interface is investigated by electron back-scattering diffraction (EBSD; TSL OIM analysis 7.3) analysis. On the basis of the results obtained by EDS and EBSD, the reaction phases of the Cu/ Al_3Ti interface are identified.

3. Results and discussion

3.1 Cu/ Al_3Ti diffusion couple specimen

Figure 3 shows the XRD pattern of the crushed particles, indicating the presence of the tetragonal D0_{22} Al_3Ti phase. After the SPS process to obtain bulk-shaped Al_3Ti and the SPS bonding process to obtain the Cu/ Al_3Ti diffusion couple specimen, the tetragonal D0_{22} structure is still observed. The Cu/ Al_3Ti diffusion couple specimen with the tetragonal D0_{22} Al_3Ti phase can be fabricated by the SPS route.

The cross-sectional SEM morphologies at the interface between Cu and Al₃Ti in the Cu/Al₃Ti diffusion couple specimen before heat treatment are shown in Figs. 4(a)-4(d), for which bonding is carried out at 600 °C for 300 s, at 600 °C for 600 s, at 700 °C for 600 s, and at 800 °C for 600 s, respectively. No reaction was found at the interface region for the Cu/Al₃Ti diffusion couple specimen obtained by SPS carried out at 600 °C for 300 s, as shown in Fig. 4(a). Therefore, the initial Cu/Al₃Ti diffusion couple specimen without the formation of the Al_{2.5}Cu_{0.5}Ti phase can be obtained by SPS at a lower sintering temperature for a shorter sintering time. On the other hand, some reaction layers are formed at the Cu/Al₃Ti interface during sintering at a higher sintering temperature for a longer sintering time, as shown in Figs. 4(b)-4(d). The results of EDS analysis are listed in Table I. As can be seen, one of the layers that appeared in Figs. 4(b)-4(d) has a nearly stoichiometric composition of the Al_{2.5}Cu_{0.5}Ti phase. It is speculated that Cu atoms can diffuse into the Al₃Ti phase to form an Al_{2.5}Cu_{0.5}Ti phase. The thicknesses of the Al_{2.5}Cu_{0.5}Ti layer, x , in the specimens obtained at 600, 700, and 800 °C for 600 s are 2.3, 13.6, and 67.1 μm, respectively. In this way, with increasing SPS temperature, the thickness of the Al_{2.5}Cu_{0.5}Ti layer, x , increases significantly.

Figures 5(a)-5(e) show SEM images of the Cu/Al₃Ti interface in the Cu/Al₃Ti diffusion couple specimens heated at 600 °C for 0.5, 1.0, 2.0, 4.0, and 8.0 h, respectively. The gray, dark gray, and dark regions shown in the images correspond to Cu, formed layers and Al₃Ti, respectively. The EDS results are listed in Table II, which shows that the composition of one of the formed layers is also close to that of Al_{2.5}Cu_{0.5}Ti. The Al_{2.5}Cu_{0.5}Ti layer was formed on the Al₃Ti side rather than on the Cu side. Cu atoms diffuse into the Al₃Ti phase and replace some of the Al atoms in the Al₃Ti phase. Moreover, diffusion along the grain boundary is also observed, especially on the Al₃Ti side. The Al_{2.5}Cu_{0.5}Ti layer gradually thickens with heating time. Under the heating condition of 600 °C for 0.5, 1.0, 2.0, 4.0, and 8.0 h, the thickness of the Al_{2.5}Cu_{0.5}Ti layer formed in the bonded Cu/Al₃Ti samples was found to be 4.7, 6.1, 7.3, 9.9, and 15.6 μm, respectively.

The thickness of a reaction layer in the diffusion couples can be generally expressed by a simple parabolic equation.³⁰⁻³³⁾ At a given temperature, the dependence of the layer thickness x on heating time t can be described by the following simple empirical relationship:

$$x = k t^n, \quad (1)$$

$$\ln x = \ln k + n \ln t, \quad (2)$$

where k is the growth rate constant and n is the kinetic exponent. A kinetic exponent, n , of 0.5 suggests standard diffusion limited growth, while an n larger than 0.5 indicates interface controlled growth.³³⁾ Taking Eq. (2) into account, the relationship between $\ln x$ and $\ln t$ is obtained; the results are shown in Fig. 6. Note that $\ln x$ vs $\ln t$ shows a linear relationship. The kinetic exponent n is found to be 0.42. Therefore, the formation of the $\text{Al}_{2.5}\text{Cu}_{0.5}\text{Ti}$ layer is mainly controlled by diffusion.

To confirm that the reaction phase at the $\text{Cu}/\text{Al}_3\text{Ti}$ interface is the $\text{Al}_{2.5}\text{Cu}_{0.5}\text{Ti}$ phase, the distribution of the crystal structure around the interface is investigated for the $\text{Cu}/\text{Al}_3\text{Ti}$ diffusion couple specimen heated at 600 °C for 4.0 h. In this measurement, the L_{12} and fcc structures are detected as cubic structures, since the crystal structures of the L_{12} $\text{Al}_{2.5}\text{Cu}_{0.5}\text{Ti}$ phase and Cu are quite similar. An SEM image, an inverse pole figure (IPF) map, and a phase map of the specimen are shown in Figs. 7(a)-7(c), respectively. As shown in Fig. 7, the crystal structure of the reaction phase found on the Al_3Ti side has a cubic structure. In addition, the reaction phase has the composition of $\text{Al}_{2.5}\text{Cu}_{0.5}\text{Ti}$. Hence, it is natural to conclude that the reaction phase is an L_{12} modified $\text{Al}_{2.5}\text{Cu}_{0.5}\text{Ti}$ phase, which may be formed by the replacement of some of the Al atoms in the Al_3Ti phase by diffused Cu atoms.

3.2 Crushed particle dispersed specimen

Back-scattering electron (BSE) images showing the cross-sectional morphologies of crushed particle dispersed specimens fabricated by SPS at 500, 600, and 700 °C before heat treatment are shown in Figs. 8(a)-8(c), respectively. As can be seen from these figures, granular Al_3Ti particles are successfully embedded homogeneously in the Cu matrix. The magnified microstructures and EDS results of the above specimens are shown in Figs. 8(a')-8(c'), and Table III, respectively. No significant reaction between the Al_3Ti particle and the Cu matrix occurs at the interface in the specimen obtained by SPS at 500 °C, as shown in Fig. 8(a'). The initial crushed particle dispersed specimen without the $\text{Al}_{2.5}\text{Cu}_{0.5}\text{Ti}$ phase can be obtained by SPS at a lower SPS temperature. However, the particles in the specimens obtained by SPS at 600 and 700 °C have reaction layers, as shown in Figs. 8(b') and 8(c'), respectively. **Point 6** shown in Fig. 8(b') and point 11 shown in Fig. 8(c') have the chemical

composition of $\text{Al}_{2.5}\text{Cu}_{0.5}\text{Ti}$, as shown in Table III. This is in accordance with the Cu/ Al_3Ti diffusion couple results, which show that $\text{Al}_{2.5}\text{Cu}_{0.5}\text{Ti}$ is the main compound that can be observed at the Cu/ Al_3Ti interface. The thickness of the $\text{Al}_{2.5}\text{Cu}_{0.5}\text{Ti}$ layer increases with increasing SPS temperature and is 3.2 μm for the specimen obtained by SPS at 600 °C and 12.3 μm for that obtained by SPS at 700 °C.

Heat treatment at 600 °C is carried out for the crushed particle dispersed specimen obtained by SPS at 500 °C. Figure 9 shows a set of IPF and phase maps of the granular Al_3Ti particles in the crushed particle dispersed specimen heated for 0.5 h. The SEM images of the specimens heated for 0.5, 1.0, 2.0, 4.0, and 8.0 h are shown in Figs. 10(a)-10(e), respectively. The EDS results listed in Table IV are evidence of the formation of the $\text{Al}_{2.5}\text{Cu}_{0.5}\text{Ti}$ layer, except in the specimen heated for 0.5 h. Figure 9 show that granular Al_3Ti particles prepared by crushing arc-melted Al_3Ti have no grain boundary. The thickness of the $\text{Al}_{2.5}\text{Cu}_{0.5}\text{Ti}$ layer increases with increasing heating time: the thicknesses in the specimens heated for 0.5, 1.0, 2.0, 4.0, and 8.0 h are 1.3, 2.8, 5.5, and 10.5 μm , respectively. These values are smaller than those observed in the Cu/ Al_3Ti diffusion couple specimen. One of the main microstructural differences between these specimens is the grain structure of the Al_3Ti phase. As shown in Figs. 4, 5, and 7, the Al_3Ti phase in the Cu/ Al_3Ti diffusion couple specimen is polycrystal, while no grain boundary is found in the crushed Al_3Ti particles, as shown in Fig. 9. It is known that the grain boundary and dislocations provide extra diffusion channels. If grain boundary diffusion is significant, the reaction between Al_3Ti and Cu is accelerated. This is the case for the Cu/ Al_3Ti diffusion couple specimen. On the other hand, the crushed Al_3Ti particles do not have grain boundary, as shown in Fig. 9. Therefore, a slower migration of Cu atoms in crushed Al_3Ti particles causes the formation of a thinner layer in the crushed particle dispersed specimen.

3.3 Gas-atomized particle dispersed specimen

Figure 11 shows the result of XRD analysis for gas-atomized Al_3Ti particles. In agreement with the crushed particles, the D0_{22} structure of the Al_3Ti phase was confirmed by XRD analysis.

Figures 12(a)-12(c) show the cross-sectional morphologies of gas-atomized particle dispersed specimens obtained by SPS at 500, 600, and 700 °C, respectively. Figure 12

indicates that spherical Al_3Ti particles prepared by the gas-atomization method are polycrystals. The compositions obtained by EDS analysis of SEM images are listed in Table V. It is worth noting that the progress of the reaction is found for the gas-atomized Al_3Ti particle dispersed specimens but small for the crushed Al_3Ti particle dispersed specimens shown in Figs. 8(a)-8(c). It is found that the formation of the $\text{Al}_{2.5}\text{Cu}_{0.5}\text{Ti}$ layer is mainly controlled by diffusion, which is enhanced by the presence of grain boundaries. Figures 12(b) and 12(c) also indicate that grain boundaries are important diffusion channels during the reaction, as shown by the migration of Cu atoms along grain boundaries of Al_3Ti .

When the gas-atomized Al_3Ti particle dispersed Al matrix specimens (Al-10 vol% Al_3Ti specimens) are heated at an elevated temperature, spherical Al_3Ti particles are found to be divided into smaller parts.³⁴⁾ The gas-atomized Al_3Ti particle dispersed Cu matrix specimens (Cu-10 vol% Al_3Ti specimens) obtained by SPS at 500 °C without reaction are heated at 600 °C, and the results are shown in Fig. 13. Moreover, IPF and phase maps of the specimen heated at 600 °C for 0.5 h are shown in Fig. 14. As already mentioned above, the spherical Al_3Ti particles fabricated by gas-atomization are polycrystals. No division of gas-atomized Al_3Ti particles after heating was observed when the matrix is Cu. Instead, the reaction between Al_3Ti and Cu was found, as shown in Table VI. Again, the enhanced reaction between Al_3Ti and Cu is observed in gas-atomized particle dispersed specimens, suggesting that the grain boundaries in the Al_3Ti particles are beneficial to the reaction subsequent to grain boundary diffusion. Numerous grain boundaries of gas-atomized Al_3Ti particles became diffusion paths, which results in the enhancement of the reaction between Al_3Ti and Cu.

4. Conclusions

In this study, Cu/ Al_3Ti diffusion couple specimens, specimens with crushed Al_3Ti particles dispersed in the Cu matrix (crushed particle dispersed specimens), and specimens with gas-atomized Al_3Ti particles dispersed in the Cu matrix (gas-atomized particle dispersed specimens) are fabricated by SPS. These specimens are heated at 600 °C for up to 8 h, and the reaction between Cu and Al_3Ti is studied. The main results are as follows.

- 1) The Cu/ Al_3Ti diffusion couple specimen and the specimens with Al_3Ti particles dispersed in the Cu matrix (Cu-10 vol% Al_3Ti specimen) without the $\text{Al}_{2.5}\text{Cu}_{0.5}\text{Ti}$ phase

can be obtained by SPS.

- 2) During the heat treatment, an $\text{Al}_{2.5}\text{Cu}_{0.5}\text{Ti}$ layer is formed at the $\text{Cu}/\text{Al}_3\text{Ti}$ interface in the $\text{Cu}/\text{Al}_3\text{Ti}$ diffusion couple specimen. The thickness of the $\text{Al}_{2.5}\text{Cu}_{0.5}\text{Ti}$ layer increases remarkably when the heating time is increased. The layer thickness is linear with the square root of heating time, since the formation of the $\text{Al}_{2.5}\text{Cu}_{0.5}\text{Ti}$ layer is mainly controlled by diffusion.
- 3) During the heat treatment of the crushed particle dispersed specimens, an $\text{Al}_{2.5}\text{Cu}_{0.5}\text{Ti}$ layer is formed at the interface. The thickness of the $\text{Al}_{2.5}\text{Cu}_{0.5}\text{Ti}$ layer increases with increasing heating time. Compared with the diffusion couple specimen, the crushed particle dispersed specimen with the same heat treatment showed a thin layer.
- 4) An enhanced reaction between Al_3Ti and Cu is found for gas-atomized particle dispersed specimens. This is because the gas-atomized Al_3Ti particles are polycrystals, and form numerous grain boundaries. The grain boundaries in the Al_3Ti phase are beneficial to the reaction subsequent to grain boundary diffusion.

Acknowledgments

This research was supported by the New Energy and Industrial Technology Development Organization (NEDO) of Japan, and by Japan Science and Technology Agency (JST) under the Industry-Academia Collaborative R&D Program "Heterogeneous Structure Control: Towards Innovative Development of Metallic Structural Materials". The authors are also thankful for the financial support from The Light Metal Educational Foundation Inc., Japan.

References

- 1) P. S. Mohanty and J. E. Gruzleski, *Acta Metal. Mater.* **43**, 2001 (1995).
- 2) A. Cibula, *J. Inst. Met.* **76**, 321 (1949–1950).
- 3) I. G. Davies, J. M. Dennis, and A. Hellawell, *Metall. Trans.* **1**, 275 (1970).
- 4) T. Motegi and A. Ohno, *Keikinzoku* **31**, 415 (1981) [in Japanese].
- 5) M. Easton and D. StJohn, *Metall. Mater. Trans. A* **30**, 1613 (1999).
- 6) C. T. Lee and S. W. Chen, *Mater. Sci. Eng. A* **325**, 242 (2002).

- 7) Z. Zhang, Y. Watanabe, I. Kim, X. Liu, and X. Bian, *Metall. Mater. Trans. A* **36**, 837 (2005).
- 8) Z. Zhang, S. Hosoda, I. S. Kim, and Y. Watanabe, *Mater. Sci. Eng. A* **425**, 55 (2006).
- 9) H. Sato, K. Ota, H. Kato, M. Furukawa, M. Azuma, Y. Watanabe, Z. Zhang, and K. Tsuzaki, *Mater. Trans.* **54**, 1554 (2013).
- 10) JCPDS No. 04-0787.
- 11) JCPDS No. 26-0039.
- 12) K. Honda, K. Ushioda, W. Yamada, K. Tanaka, and H. Hatanaka, *Mater. Trans.* **49**, 1401 (2008).
- 13) K. Yamauchi, T. Kunimine, H. Sato, and Y. Watanabe, *Mater. Trans.* **56**, 99 (2015).
- 14) Y. Watanabe, Q. Zhou, H. Sato, T. Fujii, and T. Inamura, *Jpn. J. Appl. Phys.* **56**, 01AG01 (2017).
- 15) J. Tarnacki and Y.-W. Kim, *Scr. Metall.* **22**, 329 (1988).
- 16) M. B. Winnicka and R. A. Varin, *Scr. Metall.* **23**, 1199 (1989).
- 17) H. Mabuchi, K. Hirukawa, H. Tsuda, and Y. Nakayama, *Scr. Metall. Mater.* **24**, 505 (1990).
- 18) H. R. P. Inoue, C. V. Cooper, L. H. Favrow, Y. Hamada, and C. M. Wayman, *MRS Proc.* **213**, 493 (1990).
- 19) U. Prakash, R. A. Buckley, H. Jones, and C. M. Sellars, *J. Mater. Sci.* **27**, 2001 (1992).
- 20) Y. Nakayama and H. Mabuchi, *Intermetallics* **1**, 41 (1993).
- 21) Y. Watanabe and H. Sato, *Keikinzoku* **64**, 157 (2014) [in Japanese].
- 22) Y. Watanabe, T. Hamada, and H. Sato, *Jpn. J. Appl. Phys.* **55**, 01AG01 (2016).
- 23) Y. Watanabe, T. Hamada, and H. Sato, *Jpn. J. Appl. Phys.*, **56**, 01AG02 (2017).
- 24) P. Villars, A. Prince, and H. Okamoto, *Handbook of Ternary Alloys Phase Diagrams* (ASM International, Materials Park, OH, 1995) Vol. 3, p. 3374.
- 25) C. Li, Z. Yuan, R. Guo, W. Xuan, Z. Ren, Y. Zhong, X. Li, H. Wang, and Q. Wang, *J. Alloys Compd.* **641**, 7 (2015).
- 26) P. Badica, G. V. Aldica, M. Burdusel, H. Borodianska, Y. Sakka, and O. Vasylykiv, *Jpn. J. Appl. Phys.* **53**, 05FB22 (2014).
- 27) N. Masahashi, S. Semboshi, K. Watanabe, Y. Higuchi, H. Yamagata, and Y. Ishizaki, *J. Mater. Sci.* **48**, 5801 (2013).
- 28) Z. Zhang, X. Shen, C. Zhang, S. Wei, S. Lee, and F. Wang, *Mater. Sci. Eng. A* **565**, 326

(2013).

29) Y. J. Wu, R. Kimura, N. Uekawa, K. Kakegawa, and Y. Sasaki, *Jpn. J. Appl. Phys.* **41**, L219 (2002).

30) D.-G. Kim, J.-W. Yoon, C.-Y. Lee, and S.-B. Jung, *Mater. Trans.* **44**, 72 (2003).

31) M. Kajihara, *Mater. Trans.* **47**, 1480 (2006).

32) L. Xu, Y. Y. Cui, Y. L. Hao, and R. Yang, *Mater. Sci. Eng. A* **435-436**, 638 (2006).

33) M. Mirjalili, M. Soltanieh, K. Matsuura, and M. Ohno, *Intermetallics* **32**, 297 (2013).

34) Y. Watanabe, T. Hirako, T. Chiba, and H. Sato, *Keikinzoku* **67**, 208 (2017) [in Japanese].

Figure caption list

Fig. 1. (Color online) Al-Ti-Cu ternary alloy phase diagram cited from Ref. 24.

Fig. 2. (Color online) Flow diagram for fabrication of Cu/Al₃Ti diffusion couple specimens.

Fig. 3. (Color online) XRD profile of crushed Al₃Ti particles.

Fig. 4. (Color online) SEM images of microstructures of Cu/Al₃Ti diffusion couple specimens bonded at 600 °C for 300 s (a), at 600 °C for 600 s (b), at 700 °C for 600 s (c), and at 800 °C for 600 s (d) without heat treatment.

Fig. 5. (Color online) SEM images of microstructures of Cu/Al₃Ti interface in the Cu/Al₃Ti diffusion couple specimens heated at 600 °C for 0.5 (a), 1 (b), 2 (c), 4 (d), and 8 (e) h. SPS bonding was carried out at 600 °C for 300 s.

Fig. 6. (Color online) Relationship between thickness of Al_{2.5}Cu_{0.5}Ti layer and heating time. Note that this figure is plotted using a log-log plot.

Fig. 7. (Color Online) (a) SEM image showing microstructure around Cu/Al₃Ti interface in the specimen heated at 600 °C for 4 h. (b) and (c) show the IPF map and phase map of the white rectangular region shown in (a), respectively.

Fig. 8. (Color online) BSE images of microstructures of crushed particle dispersed specimens obtained by SPS at 500 °C (a) and (a'), 600 °C (b) and (b'), and 700 °C (c) and (c') without heat treatment.

Fig. 9. (Color Online) IPF and phase maps of granular Al₃Ti particles in the crushed particle dispersed specimen heated at 600 °C for 0.5 h.

Fig. 10. (Color online) SEM images of microstructures of crushed particle dispersed specimens heated at 600 °C for 0.5 (a), 1 (b), 2 (c), 4 (d), and 8 (e) h.

Fig. 11. (Color online) XRD profile of gas-atomized Al₃Ti particles.

Fig. 12. (Color online) SEM images of microstructures of gas-atomized particle dispersed specimens obtained by SPS at 500 °C (a) and (a'), 600 °C (b) and (b'), and 700 °C (c) and (c') without heat treatment.

Fig. 13. (Color online) SEM images of microstructures of gas-atomized particle dispersed specimens heated at 600 °C for 0.5 (a), 1 (b), 2 (c), 4 (d), and 8 (e) h.

Fig. 14. (Color Online) IPF and phase maps of gas-atomized Al₃Ti particles in the gas-atomized particle dispersed specimen heated at 600 °C for 0.5 h.

Table I. Compositional analysis of the Cu/Al₃Ti interface in Cu/Al₃Ti diffusion couple specimen without heat treatment, shown in Fig. 4 (mol%).

	Al	Cu	Ti
Theoretical value of Al _{2.5} Cu _{0.5} Ti	62.5	12.5	25.0
1 [Cu side in Fig. 4(b)]	0.05	99.29	0.66
2 [Cu side in Fig. 4(b)]	18.11	81.89	0.00
3 [Cu side in Fig. 4(b)]	19.72	80.28	0.00
4 [Cu side in Fig. 4(b)]	31.56	67.93	0.51
5 [Cu side in Fig. 4(b)]	30.39	69.61	0.00
6 [Al ₃ Ti side in Fig. 4(b)]	72.01	0.00	27.99
7 [Cu side in Fig. 4(c)]	0.00	99.60	0.40
8 [Reaction layer in Fig. 4(c)]	19.92	79.56	0.52
9 [Reaction layer in Fig. 4(c)]	22.57	56.03	21.40
10 [Reaction layer in Fig. 4(c)]	61.55	13.13	25.32
11 [Al ₃ Ti side in Fig. 4(c)]	73.08	0.53	26.39
12 [Cu side in Fig. 4(d)]	0.00	99.79	0.21
13 [Reaction layer in Fig. 4(d)]	17.59	81.95	0.47
14 [Reaction layer in Fig. 4(d)]	19.58	57.75	22.67
15 [Reaction layer in Fig. 4(d)]	58.92	15.81	25.28
16 [Reaction layer in Fig. 4(d)]	58.90	16.06	25.05
17 [Reaction layer in Fig. 4(d)]	62.99	10.65	26.35
18 [Al ₃ Ti side in Fig. 4(d)]	72.12	0.18	27.71

Table II. Compositional analysis of Cu/Al₃Ti interface in the Cu/Al₃Ti diffusion couple specimens heated at 600 °C, shown in Fig. 5 (mol%).

	Al	Cu	Ti
Theoretical value of Al _{2.5} Cu _{0.5} Ti	62.5	12.5	25.0
1 [Cu side in Fig. 5(a)]	0.00	100.00	0.00
2 [Cu side in Fig. 5(a)]	27.34	71.95	0.70
3 [Reaction layer in Fig. 5(a)]	61.56	14.10	24.34
4 [Al ₃ Ti side in Fig. 5(a)]	71.00	0.09	28.91
5 [Cu side in Fig. 5(b)]	0.00	99.68	0.32
6 [Cu side in Fig. 5(b)]	27.75	71.75	0.49
7 [Reaction layer in Fig. 5(b)]	22.65	61.20	16.15
8 [Reaction layer in Fig. 5(b)]	61.93	12.98	25.09
9 [Cu side in Fig. 5(c)]	4.68	95.27	0.05
10 [Reaction layer in Fig. 5(c)]	27.83	71.84	0.33
11 [Reaction layer in Fig. 5(c)]	44.26	41.05	14.69
12 [Reaction layer in Fig. 5(c)]	59.36	15.04	25.6
13 [Al ₃ Ti side in Fig. 5(c)]	72.02	0.08	27.9
14 [Cu side in Fig. 5(d)]	0.04	99.57	0.39
15 [Reaction layer in Fig. 5(d)]	22.66	76.84	0.49
16 [Reaction layer in Fig. 5(d)]	43.12	40.51	16.37
17 [Reaction layer in Fig. 5(d)]	60.27	14.74	24.98
18 [Al ₃ Ti side in Fig. 5(d)]	72.45	0.00	27.55
19 [Reaction layer in Fig. 5(e)]	23.55	76.24	0.20
20 [Reaction layer in Fig. 5(e)]	42.51	40.46	17.02
21 [Reaction layer in Fig. 5(e)]	60.85	12.79	26.35

Table III. Compositional analysis of crushed particle dispersed specimens before heat treatment shown in Fig. 8 (mol%).

	Al	Cu	Ti
Theoretical value of $\text{Al}_{2.5}\text{Cu}_{0.5}\text{Ti}$	62.5	12.5	25.0
1 [Matrix in Fig. 8(a')]	0.18	99.19	0.63
2 [Matrix in Fig. 8(a')]	0.00	100.00	0.00
3 [Particle in Fig. 8(a')]	71.39	0.84	27.76
4 [Matrix in Fig. 8(b')]	0.57	99.43	0.00
5 [Reaction layer in Fig. 8(b')]	20.40	60.79	18.81
6 [Reaction layer in Fig. 8(b')]	61.20	13.18	25.62
7 [Particle in Fig. 8(b')]	72.30	0.56	27.15
8 [Matrix in Fig. 8(c')]	0.00	99.67	0.33
9 [Reaction layer in Fig. 8(c')]	18.21	81.38	0.41
10 [Reaction layer in Fig. 8(c')]	20.64	61.32	18.04
11 [Reaction layer in Fig. 8(c')]	61.59	13.12	25.29
12 [Particle in Fig. 8(c')]	72.18	0.61	27.20

Table IV. Compositional analysis of crushed particle dispersed specimens heated at 600 °C, shown in Fig. 10 (mol%).

	Al	Cu	Ti
Theoretical value of $Al_{2.5}Cu_{0.5}Ti$	62.5	12.5	25.0
1 [Matrix in Fig. 10(a)]	0.24	99.47	0.29
2 [Particle in Fig. 10(a)]	75.65	0.53	23.83
3 [Particle in Fig. 10(a)]	73.95	0.02	26.03
4 [Particle in Fig. 10(a)]	75.16	0.51	24.33
5 [Reaction layer in Fig. 10(b)]	60.41	12.48	27.11
6 [Reaction layer in Fig. 10(b)]	61.31	11.36	27.33
7 [Particle in Fig. 10(b)]	72.07	0.33	27.60
8 [Particle in Fig. 10(b)]	72.59	0.00	27.41
9 [Matrix in Fig. 10(c)]	0.00	99.56	0.44
10 [Reaction layer in Fig. 10(c)]	62.24	14.18	23.59
11 [Reaction layer in Fig. 10(c)]	62.54	12.79	24.67
12 [Particle in Fig. 10(c)]	73.07	0.00	26.93
13 [Reaction layer in Fig. 10(d)]	62.87	12.02	25.12
14 [Reaction layer in Fig. 10(d)]	61.03	13.14	25.82
15 [Particle in Fig. 10(d)]	72.82	0.00	27.18
16 [Particle in Fig. 10(d)]	73.12	0.30	26.58
17 [Reaction layer in Fig. 10(e)]	21.24	66.29	12.46
18 [Reaction layer in Fig. 10(e)]	60.65	13.22	26.13
19 [Reaction layer in Fig. 10(e)]	61.44	12.58	25.98
20 [Particle in Fig. 10(e)]	72.10	0.49	27.41

Table V. Compositional analysis of gas-atomized particle dispersed specimens before heat treatment shown in Fig. 12 (mol%).

	Al	Cu	Ti
Theoretical value of $\text{Al}_{2.5}\text{Cu}_{0.5}\text{Ti}$	62.5	12.5	25.0
1 [Matrix in Fig. 12(a')]	0.00	100.00	0.00
2 [Particle in Fig. 12(a')]	72.25	0.17	27.59
3 [Particle in Fig. 12(a')]	72.66	0.00	27.34
4 [Matrix in Fig. 12(b')]	0.00	100.00	0.00
5 [Reaction layer in Fig. 12(b')]	18.25	81.75	0.00
6 [Particle in Fig. 12(b')]	70.69	2.12	27.18
7 [Matrix in Fig. 12(c')]	0.00	100.00	0.00
8 [Reaction layer in Fig. 12(c')]	14.62	85.17	0.21
9 [Reaction layer in Fig. 12(c')]	20.31	60.46	19.24
10 [Particle in Fig. 12(c')]	61.90	12.59	25.51

Table VI. Compositional analysis of gas-atomized particle dispersed specimens heated at 600 °C, shown in Fig. 13 (mol%).

	Al	Cu	Ti
Theoretical value of Al _{2.5} Cu _{0.5} Ti	62.5	12.5	25.0
1 [Matrix in Fig. 13(a)]	0.29	99.34	0.37
2 [Particle in Fig. 13(a)]	70.57	3.09	26.35
3 [Particle in Fig. 13(a)]	71.68	0.85	27.47
4 [Particle in Fig. 13(a)]	71.18	1.18	27.63
5 [Matrix in Fig. 13(b)]	0.00	99.93	0.07
6 [Particle in Fig. 13(b)]	63.33	10.27	26.40
7 [Particle in Fig. 13(b)]	63.16	11.45	25.39
8 [Particle in Fig. 13(b)]	73.16	0.68	26.16
9 [Matrix in Fig. 13(c)]	0.77	99.23	0.00
10 [Reaction layer in Fig. 13(c)]	62.36	10.88	26.76
11 [Reaction layer in Fig. 13(c)]	61.49	12.81	25.70
12 [Core in Fig. 13(c)]	71.72	0.19	28.09
13 [Matrix in Fig. 13(d)]	0.00	100.00	0.00
14 [Reaction layer in Fig. 13(d)]	33.19	66.10	0.71
15 [Reaction layer in Fig. 13(d)]	61.54	13.54	24.92
16 [Core in Fig. 13(d)]	72.47	0.37	27.17
17 [Matrix in Fig. 13(e)]	11.78	88.22	0.00
18 [Reaction layer in Fig. 13(e)]	18.88	80.71	0.41
19 [Reaction layer in Fig. 13(e)]	59.91	15.59	24.50
20 [Core in Fig. 13(e)]	49.86	24.89	25.25

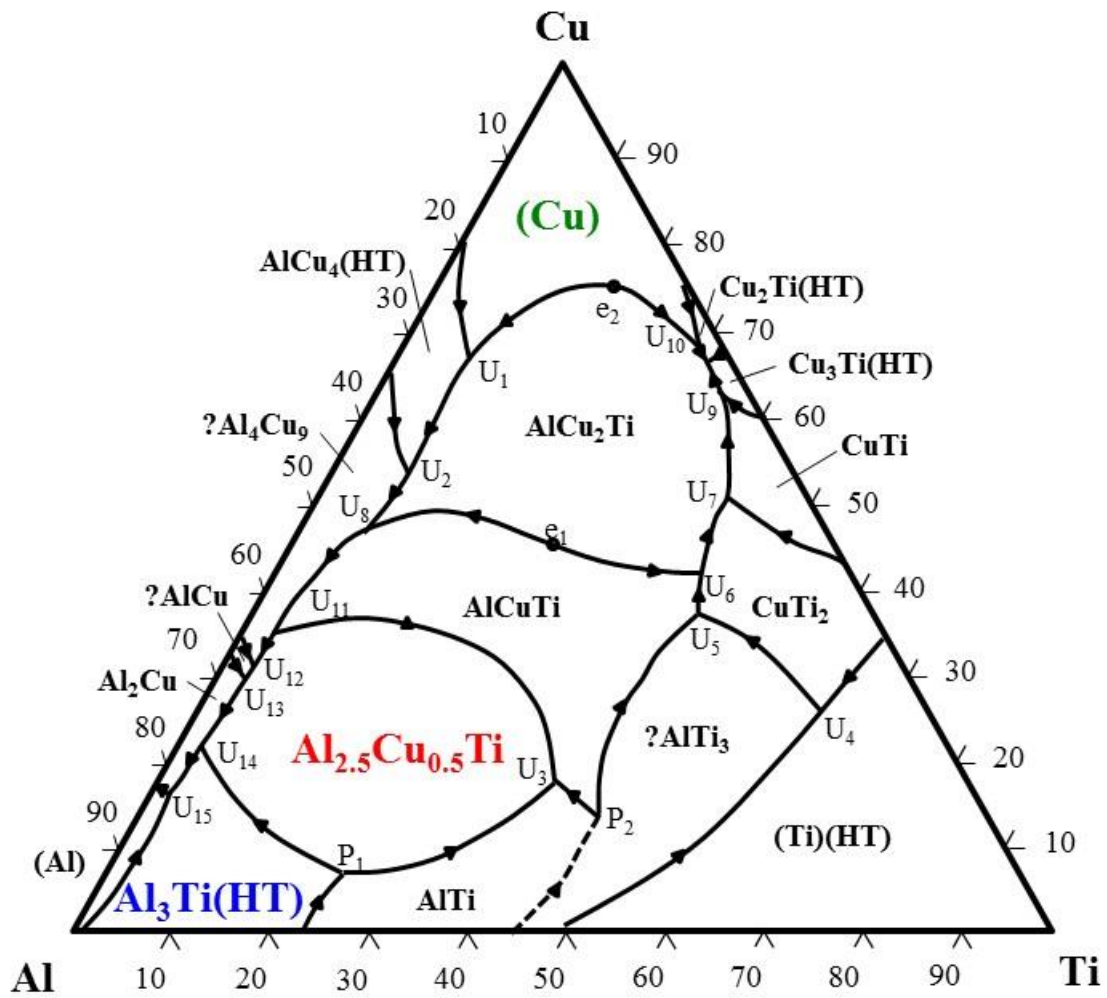


Fig. 1. (Color online) Al-Ti-Cu ternary alloy phase diagram cited from Ref. 24.

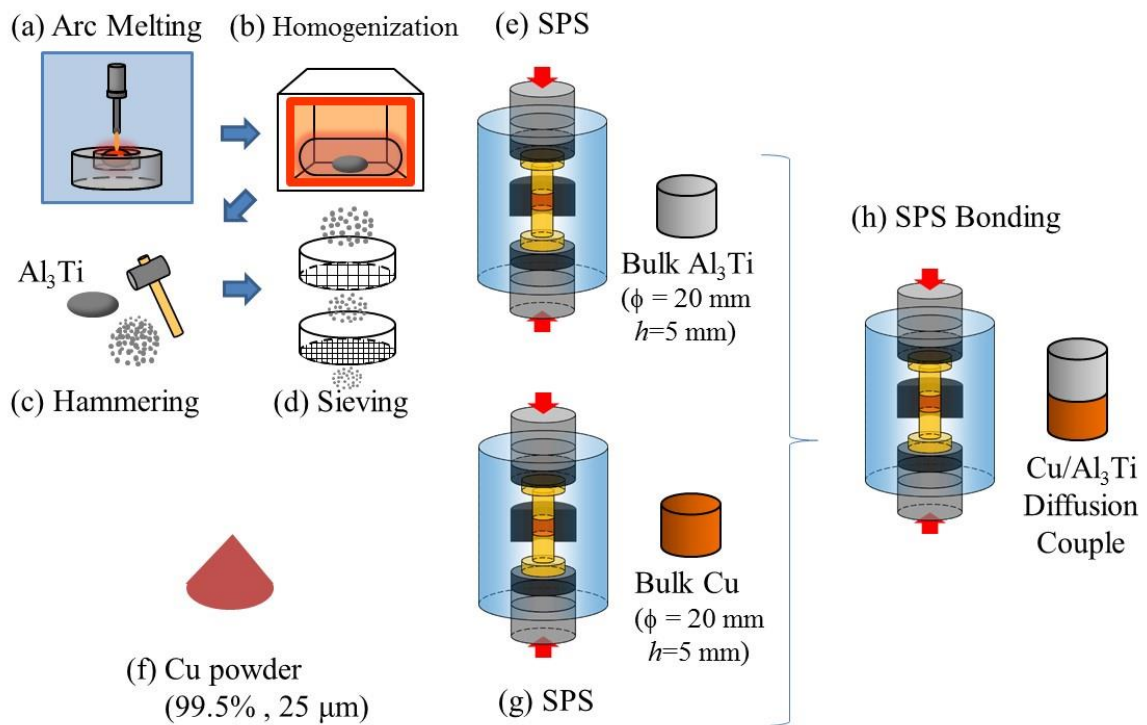


Fig. 2. (Color online) Flow diagram for fabrication of Cu/ Al_3Ti diffusion couple specimens.

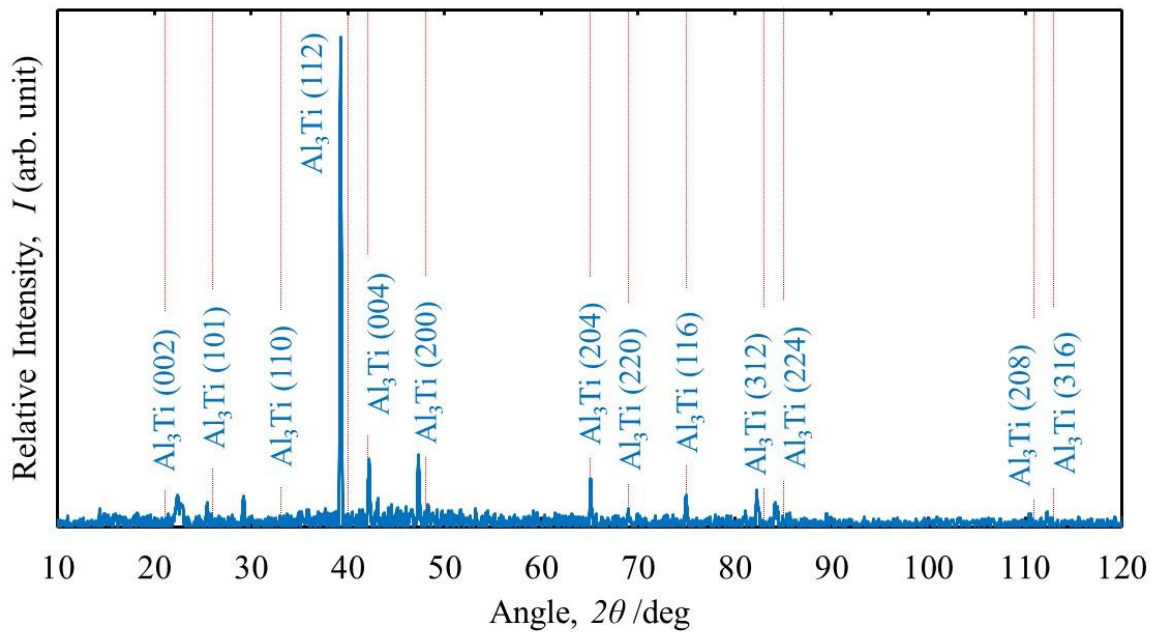


Fig. 3. (Color online) XRD profile of crushed Al_3Ti particles.

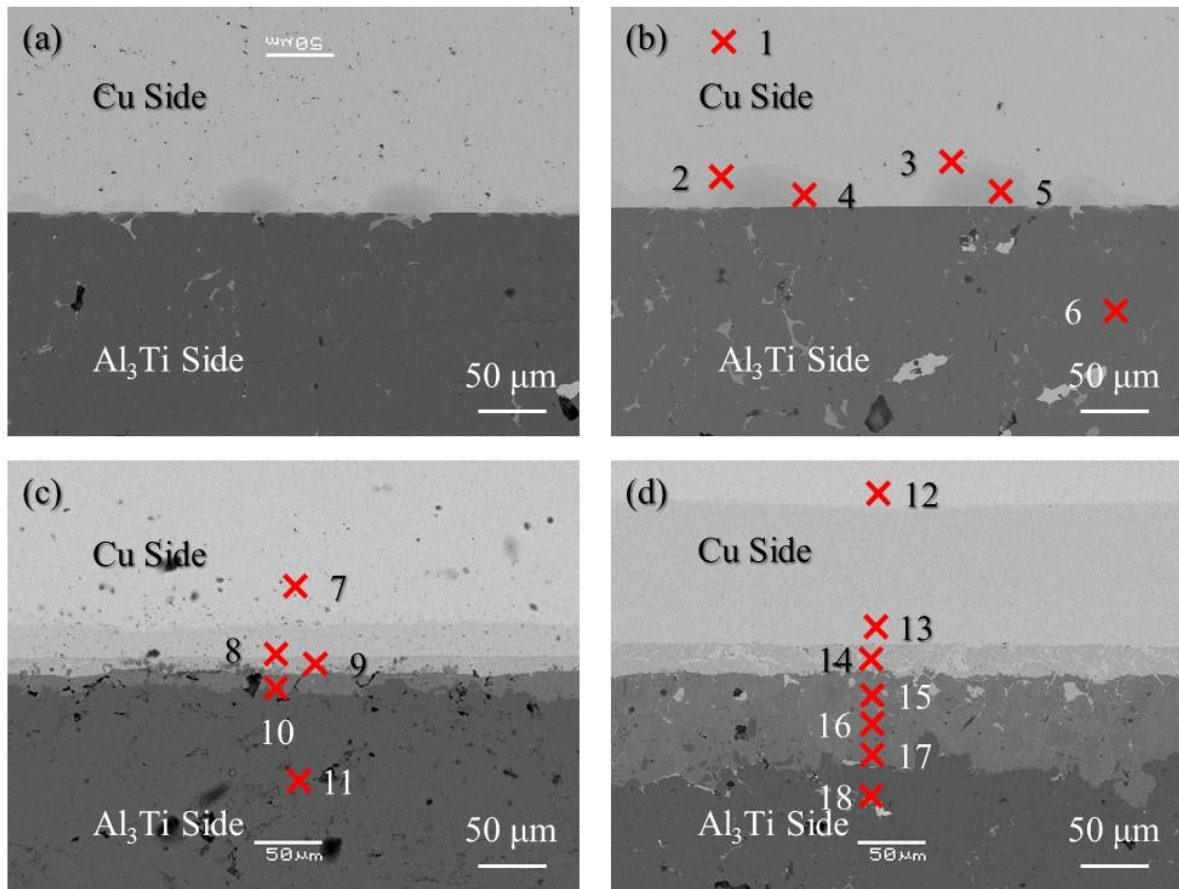


Fig. 4. (Color online) SEM images of microstructures of Cu/Al₃Ti diffusion couple specimens bonded at 600 °C for 300 s (a), at 600 °C for 600 s (b), at 700 °C for 600 s (c), and at 800 °C for 600 s (d) without heat treatment.

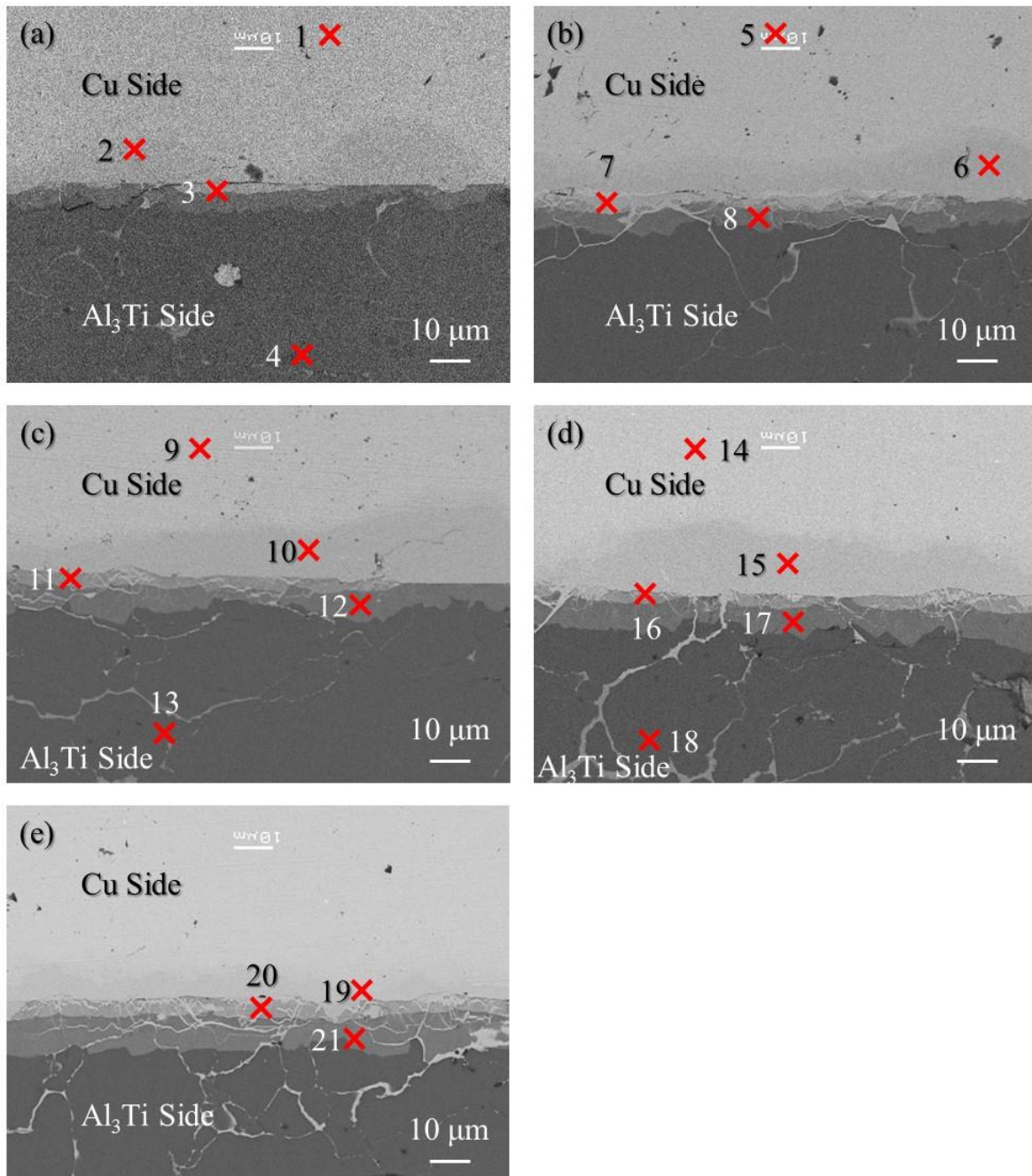


Fig. 5. (Color online) SEM images of microstructures of Cu/Al₃Ti interface in the Cu/Al₃Ti diffusion couple specimens heated at 600 °C for 0.5 (a), 1 (b), 2 (c), 4 (d), and 8 (e) h. SPS bonding was carried out at 600 °C for 300 s.

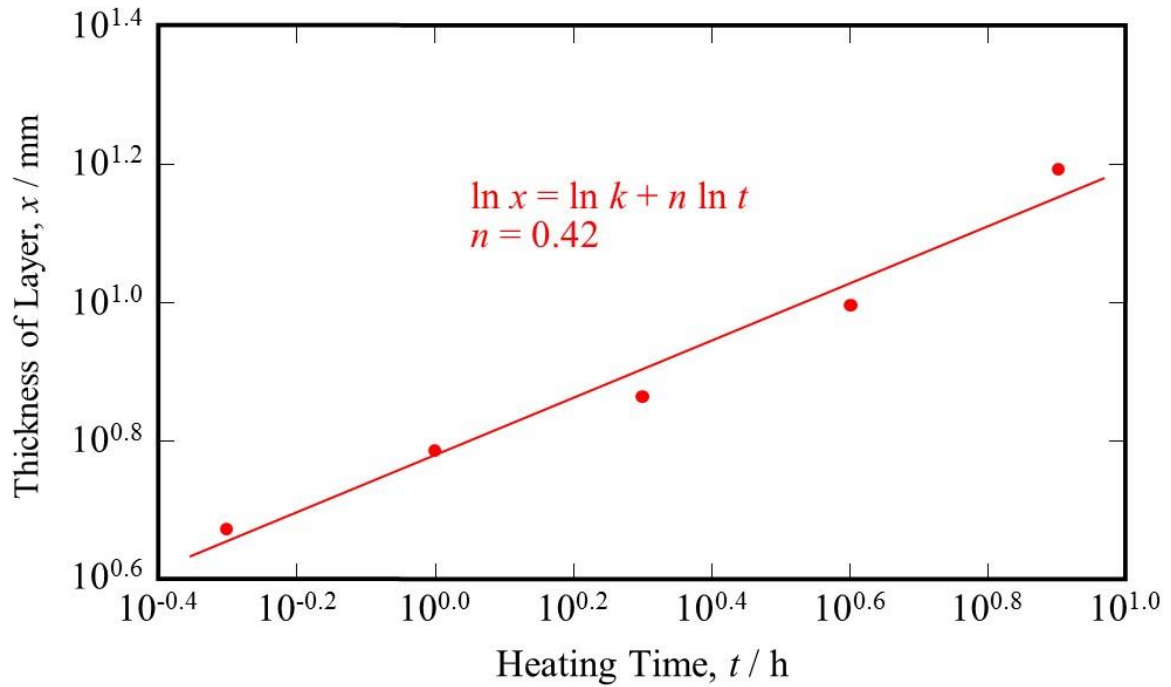


Fig. 6. (Color online) Relationship between thickness of $\text{Al}_{2.5}\text{Cu}_{0.5}\text{Ti}$ layer and heating time. Note that this figure is plotted using a log-log plot.

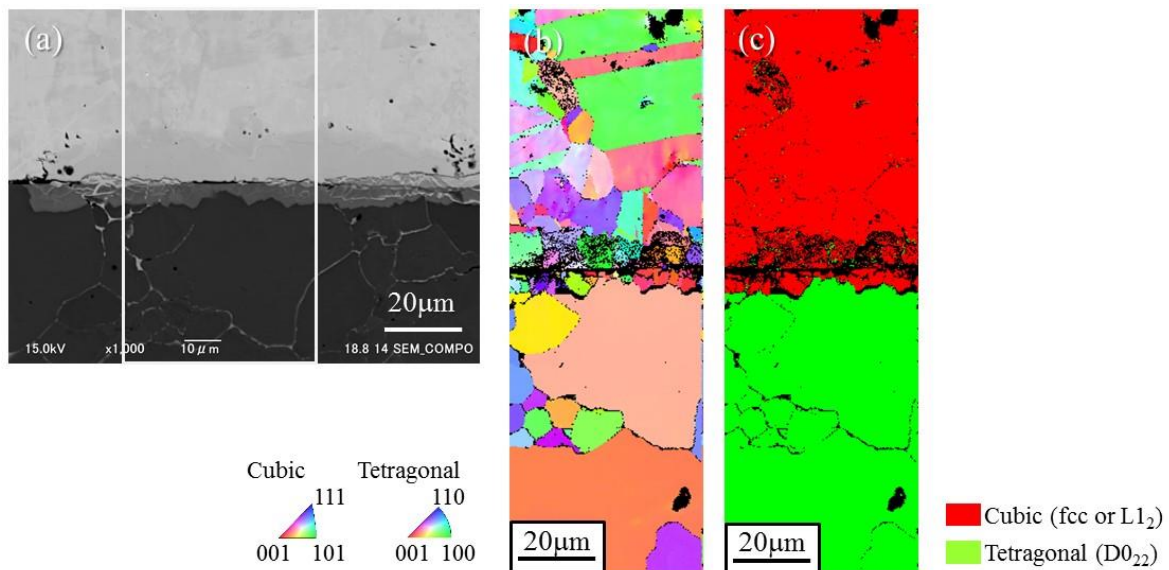


Fig. 7. (Color Online) (a) SEM image showing microstructure around $\text{Cu}/\text{Al}_3\text{Ti}$ interface in the specimen heated at 600 °C for 4 h. (b) and (c) show the IPF map and phase map of the white rectangular region shown in (a), respectively.

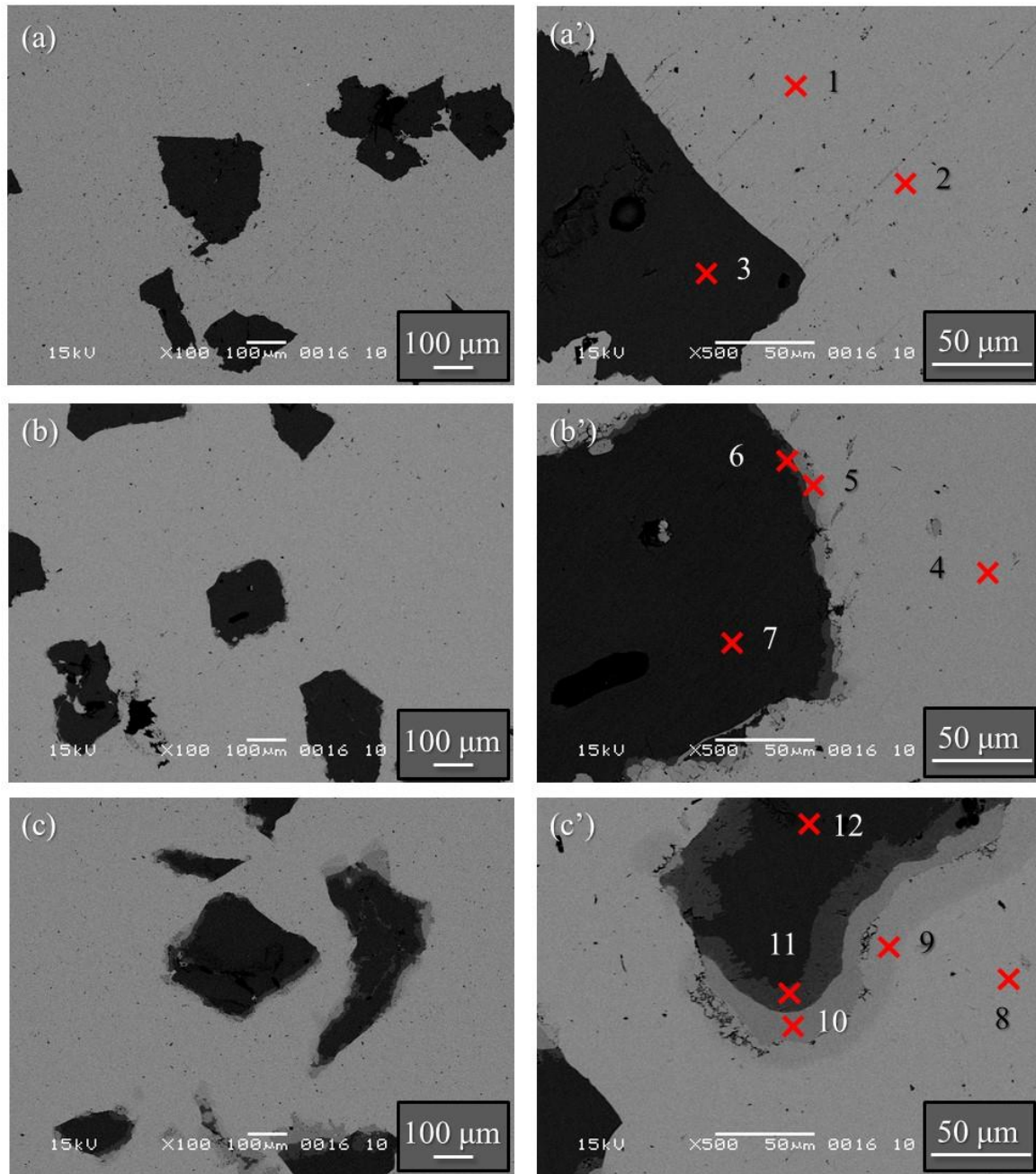


Fig. 8. (Color online) BSE images of microstructures of crushed particle dispersed specimens obtained by SPS at 500 °C (a) and (a'), 600 °C (b) and (b'), and 700 °C (c) and (c') without heat treatment.

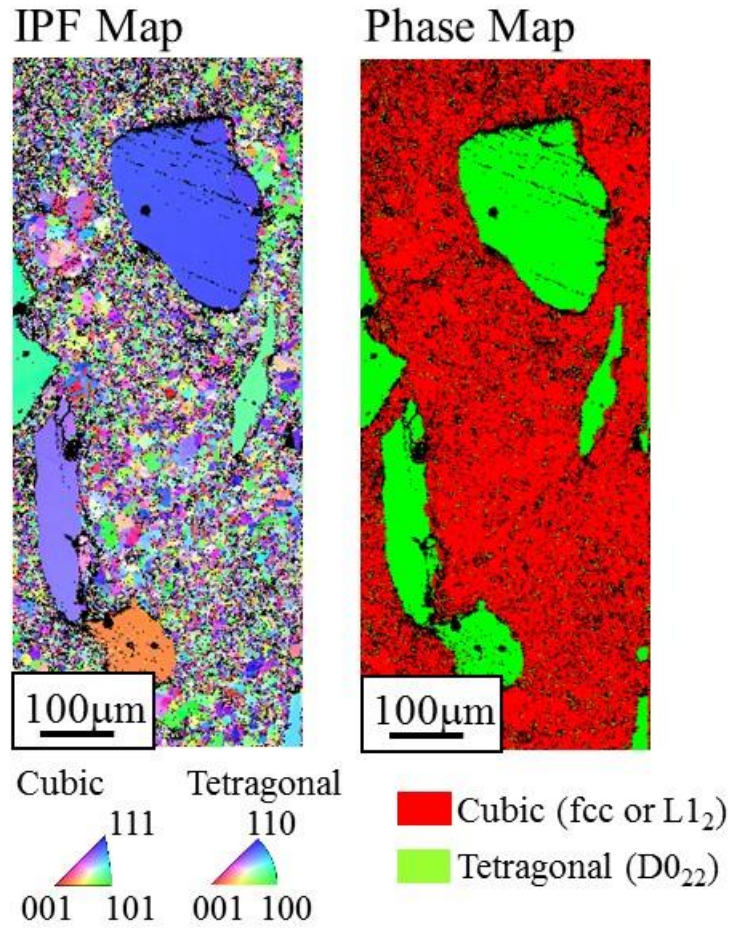


Fig. 9. (Color Online) IPF and phase maps of granular Al₃Ti particles in the crushed particle dispersed specimen heated at 600 °C for 0.5 h.

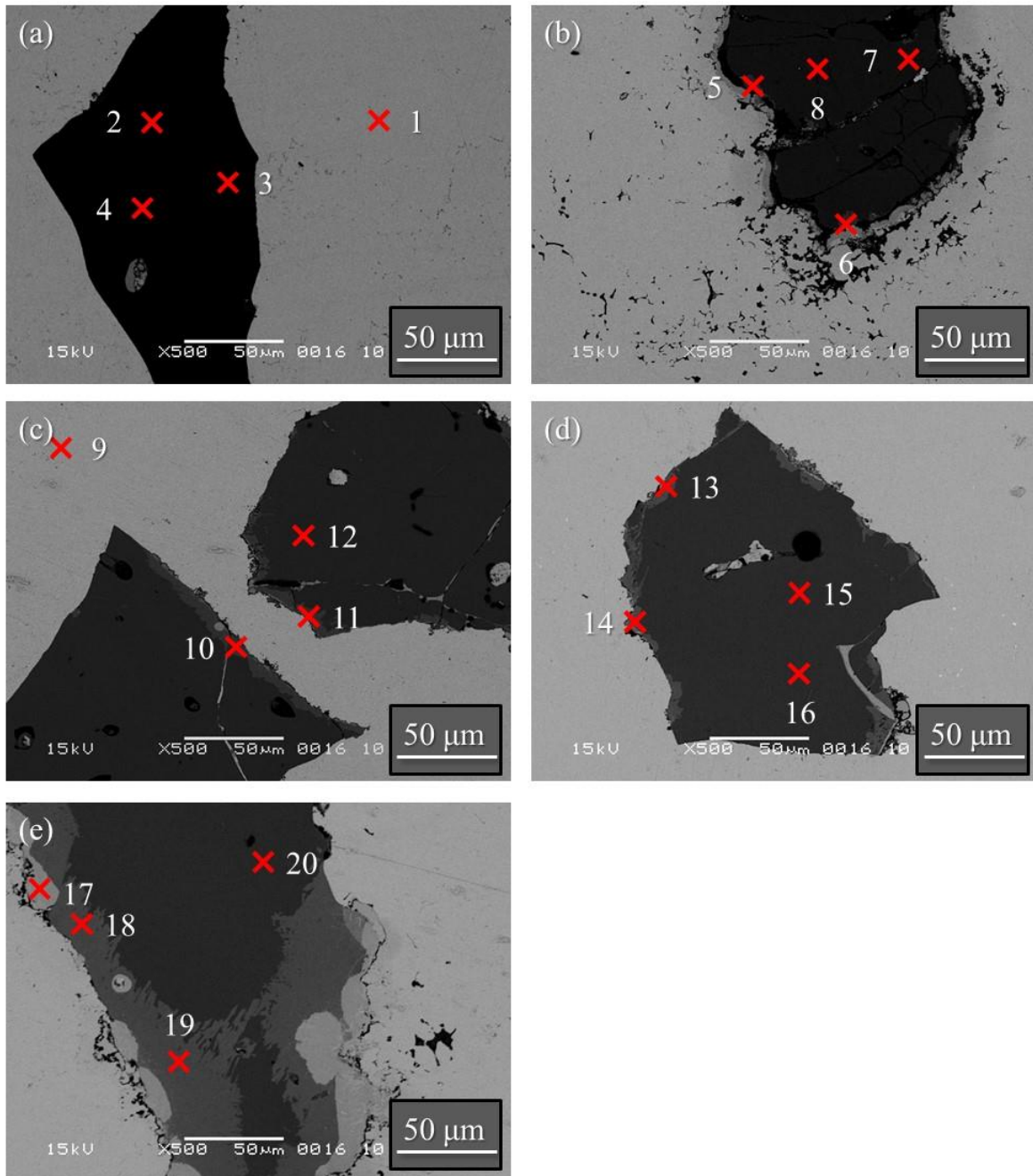


Fig. 10. (Color online) SEM images of microstructures of crushed particle dispersed specimens heated at 600 °C for 0.5 (a), 1 (b), 2 (c), 4 (d), and 8 (e) h.

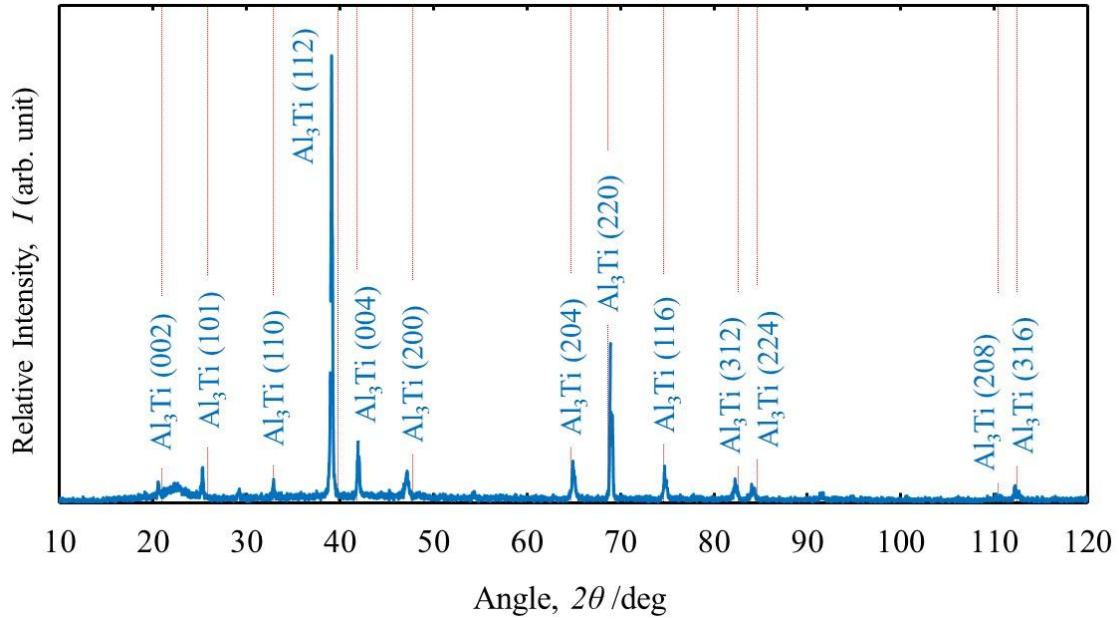


Fig. 11. (Color online) XRD profile of gas-atomized Al₃Ti particles.

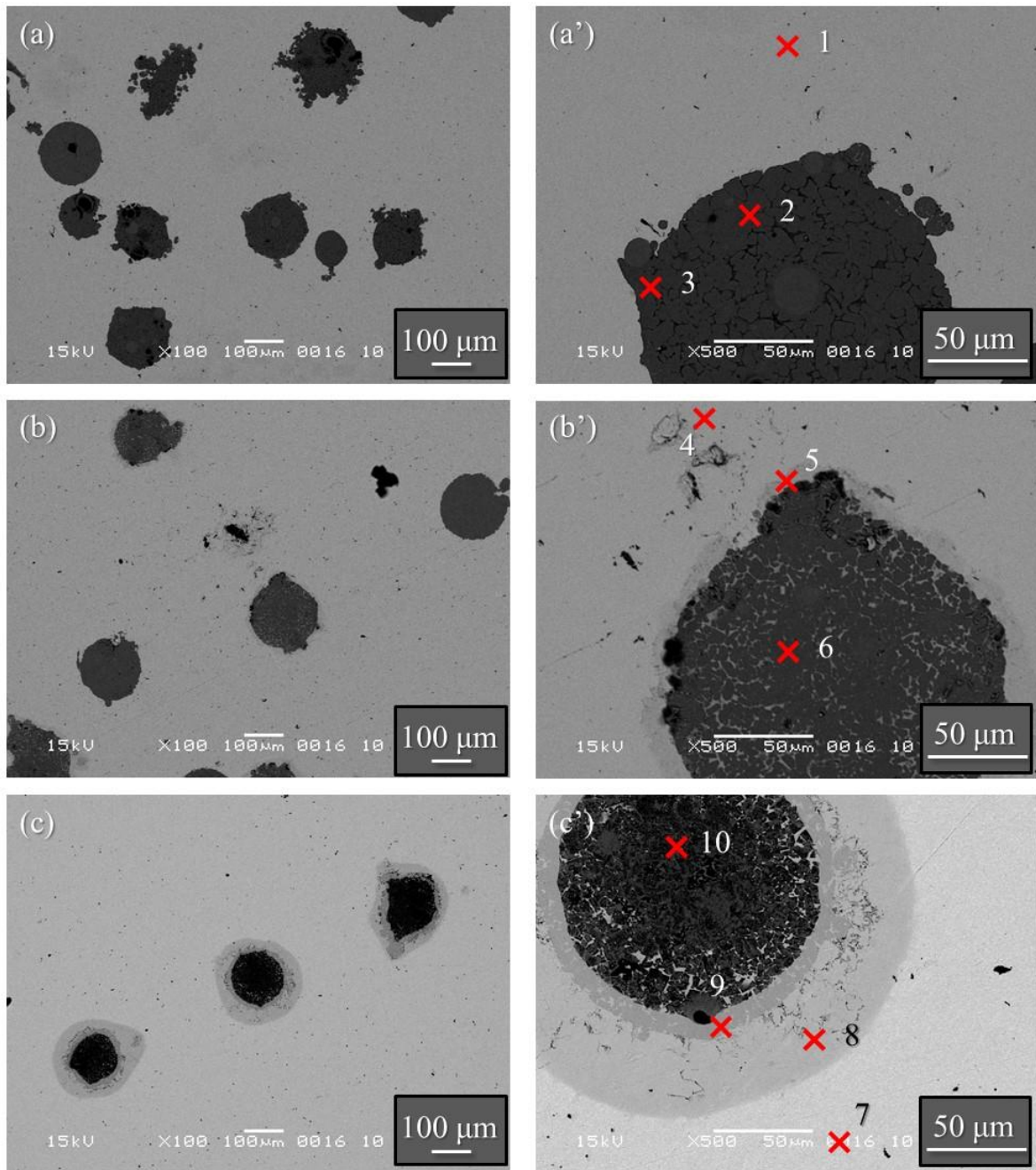


Fig. 12. (Color online) SEM images of microstructures of gas-atomized particle dispersed specimens obtained by SPS at 500 °C (a) and (a'), 600 °C (b) and (b'), and 700 °C (c) and (c') without heat treatment.

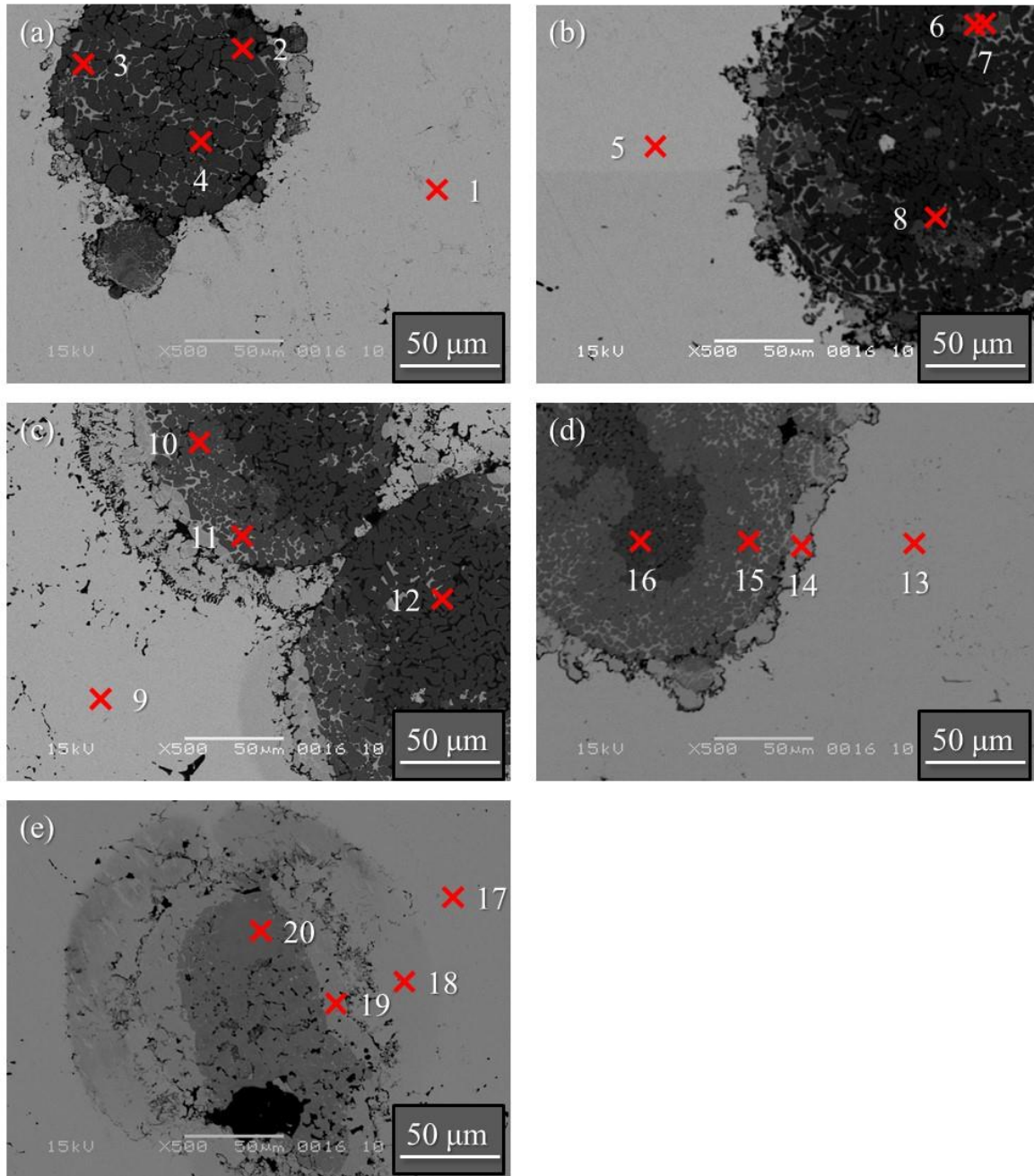


Fig. 13. (Color online) SEM images of microstructures of gas-atomized particle dispersed specimens heated at 600 °C for 0.5 (a), 1 (b), 2 (c), 4 (d), and 8 (e) h.

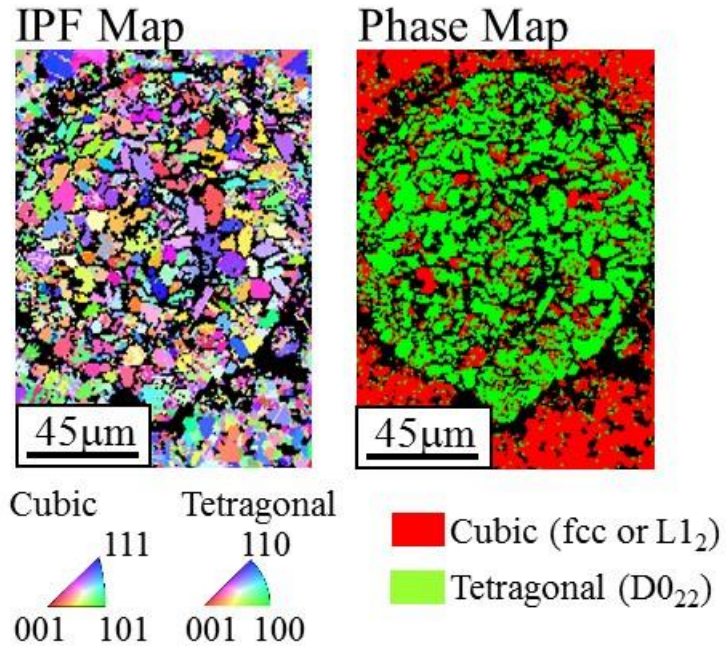


Fig. 14. (Color Online) IPF and phase maps of gas-atomized Al_3Ti particles in the gas-atomized particle dispersed specimen heated at $600\text{ }^\circ\text{C}$ for 0.5 h.